Postprint

Simulation-Based Optimization of High-Performance Wheel Loading

Koji Aoshima[1,2]**, Martin Servin**[2]**, and Eddie Wadbro**[2,3]

[1]Komatsu Ltd., Japan
[2]Umeå University, Sweden
[3]Karlstad University, Sweden

koji.aoshima@umu.se, martin.servin@umu.se, eddie.wadbro@umu.se,

Abstract -

Having smart and autonomous earthmoving in mind, we explore high-performance wheel loading in a simulated environment. This paper introduces a wheel loader simulator that combines contacting 3D multibody dynamics with a hybrid continuum-particle terrain model, supporting realistic digging forces and soil displacements at real-time performance. A total of 270,000 simulations are run with different loading actions, pile slopes, and soil to analyze how they affect the loading performance. The results suggest that the preferred digging actions should preserve and exploit a steep pile slope. High digging speed favors high productivity, while energy-efficient loading requires a lower dig speed.

Keywords -

Wheel loader; Autonomous; Simulation-Based Optimization; Multibody and soil dynamics
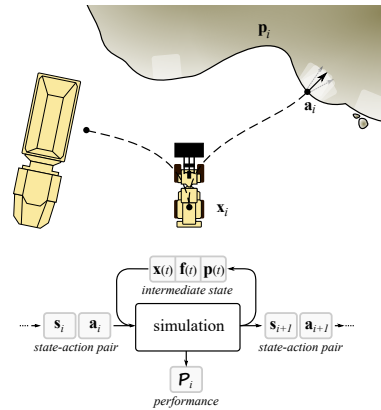
Figure 1. The typical loading cycle of filling a bucket and dumping the material in a receiver can be viewed as selecting a control action that transforms the system from one state to another with some performance that depends on the intermediate states.

1 Introduction

Smart and autonomous earthmoving equipment may significantly improve energy efficiency, productivity, and safety at construction sites and mines. If the planning and control system can be made well-informed about the physics of earthmoving operations and the current state of the environment, then it can predict the outcome of an action and select near-optimal action sequences that are well-coordinated with other systems at the site. This motivates us to explore which wheel loading actions that maximize the performance over a task. The loading task is typically operated as a repeating cycle of sequential actions: heading into a pile, scooping, breaking out of the pile, carrying the soil, and dumping it to fill bodies of dump trucks [1]. Despite the repetitive task, adjusting the loading actions to the environment for consistent high-performance loading is challenging. The difficulty lies in the complex dynamics and variability in the wheel loader-soil interaction. It is impractical to address the challenge through physical experiments. Systematic and repeatable experiments appear possible only in simulated environments, but computationally efficient models for wheel loading with realistic

soil dynamics have become available only recently.

In this paper, we introduce a method for exploring the sequential loading actions for maximum performance in a simulated environment. We view it as an optimization problem and analyze how the loading actions are expected to perform according to the situations. A simulator is developed, which combines contacting 3D multibody dynamics with a hybrid continuum-particle terrain model that supports realistic digging forces and soil displacements at real-time performance [2]. To show the ability of the simulator, we demonstrate how the loading performance depends on the pile and the loading action. In total 270,000 simulations are conducted with different action parameters for loading, pile slopes, and type of material. The performance is analyzed statistically, and some characteristic actions are compared in detail.

1.1 Related work

Some researchers have previously investigated strategies for maximizing the performance of wheel loading

in simulated environments. They especially focus on the bucket filling action, which is the most predominant action for fuel efficiency and productivity in the loading cycle [3]. Singh and Cannon [4] presented a planning algorithm to search for the best dig region and executed the planner by using a machine and pile model in 2D. Sarata et al. [5] proposed a method for dig planning, taking the 3D pile shape into account and avoiding undesirable stress by unbalanced bucket filling. Filla et al. [6, 7] investigated optimal bucket filling trajectories by using simulation based on the discrete element method (DEM), concluding that the "slicing cheese" motion, advocated by machine instructors, is indeed a good strategy. They also noted the need for fully dynamic simulation models, with the possibility to adapt the control to the changing environment as high-performing operators do, for developing optimal bucket filling strategies. The previous studies have been limited to either kinematic bucket trajectories or quasi-static soil models, often based on fundamental earthmoving equation (FEE) in combination with a cellular automata. This has several drawbacks. A kinematic bucket trajectory may not be realizable when the full dynamics and actuator force limits are taken into account. The FEE force resistance does not support situations when the vehicle or bucket is accelerating. The correct loading time and power consumption require a dynamic model. Furthermore, quasi-static soil models do not capture the actual soil displacement, around and into the bucket. This affects both the bucket fill ratio and soil spillage on the ground, which may significantly penalize the performance over time. For simulation results to be transferable to the control and planning on real sites, the dynamics of both the machine and the soil must be represented in the model. That is computationally very challenging, and few studies have been performed. Lindmark and Servin [8] explored a control strategy to maximize the loading performance using simulation based on 3D nonsmooth multibody dynamics. However, it was conducted for a load-haul-dump machine loading fragmented rock. Wheel loaders require a different strategy because of a lower breakout force than LHD:s [9] and the high-performing loading depends on the pile property [10].

1.2 Problem statement

During a loading cycle, the wheel loader typically performs a sequence of loading actions as illustrated in Figure 1. We assume that the wheel loader has a task planner and a controller for recurring *actions* $(a_i)_{i=1}^N$ during N sequential loading cycles. A loading action a_i starts with a machine state $x(t_i) \in \mathbb{R}^{N_l}$ and a pile state $p(t_i) \in \mathbb{R}^{N_p}$, which can be represented as a system *state* $s_i = [x_i, p_i] \in \mathbb{R}^{N_s}$. Then, a_i leads to some trajectory $x(t)$ and applied force $f(t)$, changing the pile state $p(t)$ over a time interval $t \in [t_i, t_i + t_{load}]$. The system ends up with a new state $s_{i+1} = [x_{i+1}, p_{i+1}]$, where p_{i+1} may include material spilled in the working area. The loading cycle can be attributed to a *performance* $\mathcal{P}_i \in \mathbb{R}^{N_{\mathcal{P}}}$. The performance depends on a state-action pair, that is, $\mathcal{P}(s_i, a_i)$. Examples of performance measures are the energy efficiency $\mathcal{P}^e = m_{load}/W$, productivity $\mathcal{P}^p = m_{load}/t_{load}$, and bucket fill ratio $\mathcal{P}^b = V/V_{bucket}$, where m_{load} is the resulting mass of the load in the bucket, $W(x, f, t_{load})$ is the accumulated work exerted by the actuators over the loading cycle of time duration t_{load}, V is the volume of the load in the bucket that has volume capacity V_{bucket}. The simulation process is illustrated in Figure 1. What is an optimal action sequence $(a_i)_{i=1}^N$ may depend on the initial pile state, p_1, and the number of loading cycles, N. For example, an optimal action sequence for $N \gtrsim 1$ may transform the pile into a poor state. That would prohibit continued loading with good performance unless the pile is restored by additional actions optimized for improving the quality. On the other hand, an optimal action sequence for over $N \to \infty$ (terminated when the pile is empty) might start with a loading performance significantly worse than what is optimal for single loadings but can maintain a good average performance. From the perspective above, optimization of N sequential loadings correspond to finding $(a_i)_{i=1}^N$ that satisfy

$$\max_{(a_i)_{i=1}^N} \sum_{i=1}^N w^\top \mathcal{P}_i \tag{1}$$

where $w \in \mathbb{R}^{N_{\mathcal{P}}}$ are weight factors for the different performance measures $\mathcal{P}$. Note that optimization over sequential loadings is not carried out in the present paper but will be pursued in future work.

2 Simulator

A simulator is created using the physics engine AGX Dynamics [11], which supports real-time simulation of multibody systems with nonsmooth contact dynamics, driveline, and deformable terrain.

2.1 Terrain model

The terrain is simulated using a multiscale hybrid model presented by Servin et al. [2]. Resting soil is modeled as a solid, discretized in a regular 3D grid and a corresponding 2D height map for the free surface that mediates contacts with earthmoving equipment. The bulk mechanical properties of the soil are parametrized by the mass density, internal friction, cohesion, and dilatancy at the bank state. When earthmoving equipment comes in contact with the terrain, a zone of active soil is predicted and resolved with particles of variable size and mass. DEM is used
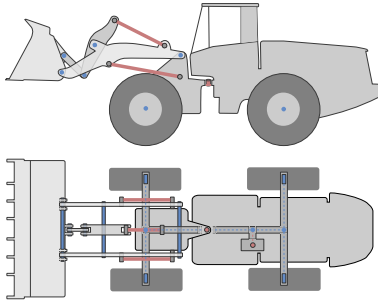
Figure 2. Overview of the wheel loader model with passive joints in blue and actuated joints in red.

Table 1. Actuators

name	type	speed range	force limit
drive	revolute	[0, 11] km/h	85 kNm
steer	revolute	[−0.1, 0.1] rad/s	100 kNm
lift	linear	[−0.2, 0.11] m/s	395 kN
tilt	linear	[−0.2, 0.1] m/s	530 kN

[13]. The actuators are controlled by specifying a momentaneous joint target speed and force limits, which are listed in Table. 1. The force limits are chosen to reflect that limited power can be drawn from the engine, which in reality supplies both the hydraulic cylinders and the driveline. In addition to the internal constraints, tire-terrain intersections give rise to frictional contact constraints, and bucket-terrain intersections cause soil failure and digging resistance. The wheel-terrain friction coefficient is set to 0.8. For clarity of the terrain dynamics, only the wheel and bucket are given visual attributes.

for particle dynamics with frictional-cohesive contact parameters and a specific mass density that matches the bulk parameters of the soil. The earthmoving equipment experiences the active soil as a low-dimensional body with the aggregated shape and inertia of the particles and with frictional-cohesive contacts at its interfaces. This can be seen as an extension of the FEE to dynamic conditions, including also bucket penetration resistance and contacts between the bucket's exterior and the surrounding soil. The multiscale model allows for combined use of a direct solver for the vehicle dynamics at high precision, an iterative solver for scalable particle dynamics at lower error tolerance, and strong coupling between the vehicle and terrain dynamics that resist soil failure when the stresses do not meet the Mohr-Coulomb criteria.

2.2 Wheel loader model

The wheel loader is modeled as a rigid multibody system consisting of a front and rear frame, connected by a revolute joint for articulated steering, four wheels, and a parallel Z-bar linkage system [12] for controlling the bucket relative to the front frame. Bucket filling is the combined effect of thrusting the vehicle into a pile, by applying torque on the wheels, while raising and tilting the bucket. The driveline model consists of a revolute motor transmitting rotational power to the front and rear wheel pairs via a main, front, and rear shaft, coupled with differentials. Each wheel is connected to the frame with a revolute joint and consists of a tire-hub pair, with finite elasticity with respect to radial, lateral, bending, and torsional displacements. The parallel Z-bar linkage system is modeled using 11 revolute and three prismatic joints, with linear motors that represent the hydraulic cylinders for raising and tilting the bucket. In total, the assembled model consists of 27 rigid bodies and 23 kinematic constraints, whereof 18 are passive joints and five are actuated. The total operating weight is 15.59 tons, wheelbase 3.030 m, and the bucket has a volume capacity of 3.0 m^3. Overall, the model roughly corresponds to a Komatsu WA320-7

2.3 Comparison with field measurements

To verify that the simulator represents the real-world counterpart, we compare the trajectories and forces of the real and simulated a wheel loader conducting a loading cycle. Data was recorded from a manually operated wheel loader and control parameters in the simulation were selected to reproduce a similar, but not identical, loading cycle. The vehicle speed, traction force, and lift and tilt cylinder forces are shown in Figure 4, and the bucket tip trajectory is in Figure 5. The forces are normalized with a characteristic force for the wheel loader. The boom and bucket angles relative to the chassis pitch. The data in Figure 4 confirms that the model is representative. The forces and trajectories do differ, e.g., the swept area of the real bucket trajectory is about 60% larger than the simulated one. This agrees with the observed difference in loaded mass and the lift force after breakout. Presumably, the discrepancy is due to differences in pile shape and soil properties, which have not been calibrated.

3 Simulations

The purpose of the simulator is to support the development of high-performance wheel loading from different pile states. Therefore, we run a large set of simulations with different action parameters and analyze their performances in relation to the pile state. Piles with four different slopes are studied: 10°, 20°, 30° and 40°. The considered soils include gravel, sand, and dirt. Following the terrain library in AGX Dynamics, they have an angle of internal friction 44°, 39°, and 40°, and dilatancy 11°, 9°, and 13°, respectively. Gravel and sand are cohesionless, while dirt has cohesion 2.1 kPa. The soils are assigned the same

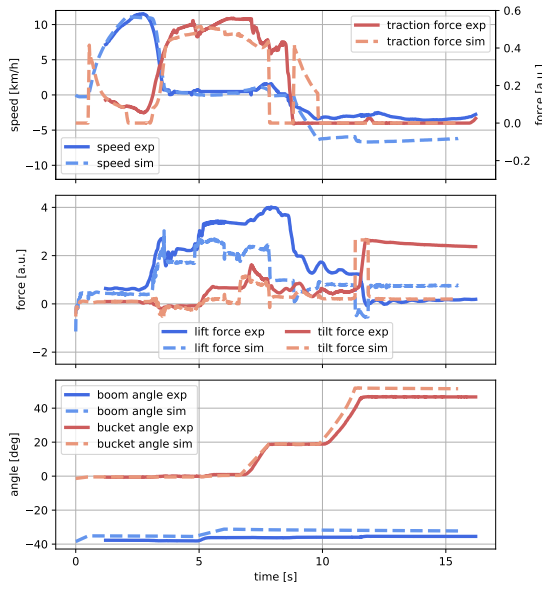Figure 3. Image sequence from field experiment and simulation.

Figure 4. Comparison of the wheel loader speed and forces during a real and simulated loading cycle.
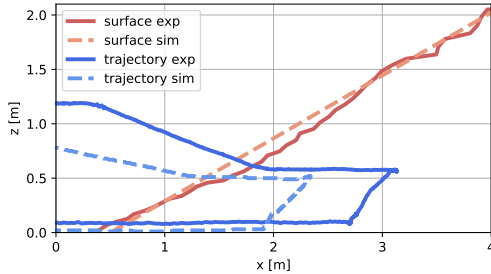

Figure 5. Comparison of the bucket tip trajectory during a real and simulated loading cycle. The pile surface is also indicated.

bulk density, 1400 kg /m^3. For simplicity, the loading scenario is restricted to entering the pile head-on, with the bucket lowered to the ground and reversing straight out after completing the loading. The loading task is controlled using eight action parameters, α_i, listed in Table 3, and discretized to 45, 000 parameter combinations per pile. In total, 270, 000 simulations were run. Loadings on sand and dirt were carried out only for piles with 30° slope.

The loading is controlled with a simplified version of admittance control [14]. The approach drive speed is $v_d = \alpha_1 v_d^{max}$, and the target speed during the penetration phase is $v_d = \alpha_2 v_d^{max}$. When the digging force exceeds the set threshold values, $F_{lift}^{dig} = \alpha_3 F_0^{dig}$ and $F_{tilt}^{dig} = \alpha_4 F_0^{dig}$, the lift and tilt actuators start running with their respective target speeds $v_{lift} = \alpha_5 v_{lift}^{max}$ and $v_{tilt} = \alpha_6 v_{tilt}^{max}$. This continues until the boom and bucket angles reach their target, $\theta_{boom} = \alpha_7$ and $\theta_{bucket} = \alpha_8$, but is aborted in case of breakout or stalling. The brake is then applied for one second, letting the activated soil come to rest. After that, the vehicle is driven in reverse at the target speed $v_d = -0.6v_d^{max}$ and with tilt target speed $v_{tilt} = 0.6v_{tilt}^{max}$ until the end position $\theta_{bucket} = 50°$ is reached. After the breakout, the lift target speed is $v_{lift} = 0.6v_{lift}^{max}$ until the end position $\theta_{boom} = -10°$ is reached. The simulation is ended when the vehicle has reversed 5 m from the entry point. The following control constants are used: $v_d^{max} = 11.0$ km/h, $v_{lift}^{max} = 0.11$ m/s, $v_{tilt}^{max} = 0.10$ m/s, and $F_0^{dig} = 100$ kN.

The simulations are run with 10 ms time-step, with the terrain discretized spatially to 0.2 m resolution, on a high-performance computer with Intel Xeon E5-2690v4 processors, each node enabling up to 28 simulations in parallel and roughly 10^4 loading cycles per CPU hour. During each simulation, the position, velocity, and force are registered over time for selected bodies, joints, and actuators. From this, the loaded mass m_{load}, dig time t_{load}, and energy consumption W are computed for each loading cycle, as well as the relative load spillage $s_{load} = V_{spill}/V_{bucket}$ of material on the ground, and the resulting pile shape. The energy efficiency and productivity performance measures, $\mathcal{P}_e$ and $\mathcal{P}_p$, are computed for each loading also.

Table 2. Action parameters

	control	values
α_1	approach speed	$[0.4, 0.6, 0.8]$
α_2	penetration speed	$[0.2, 0.4, 0.6]$
α_3	lift-trigging dig force	$[0.0, 0.3, 0.6, 0.9, 1.2]$
α_4	tilt-trigging dig force	$[0.0, 0.3, 0.6, 0.9, 1.2]$
α_5	lift speed	$[0.2, 0.4, 0.6, 0.8, 1.0]$
α_6	tilt speed	$[0.2, 0.4, 0.6, 0.8, 1.0]$
α_7	lift angle	$[-40°, -30°, -20°, -10°]$
α_8	tilt angle	$[30°, 45°]$

4 Result

Figures 6 and 7 show the variations in performance over the 270,000 simulated loading operations. The distributions over dig time, load mass, and spillage, per pile angle and material, are shown in Figure 6. In general, the trend is that the load mass increase with the slope, and the dig time is positively correlated with the load mass. The nominal dig time is around 10-12 s, which can be compared to the 15 s for completing the experimental loading cycle in Figure 4. Higher load mass requires a larger pile slope, but it is harder to achieve a high load with gravel than for sand and dirt. Spillage is mostly below 2% of the bucket volume. It increases with the pile slope and is largest for sand and smallest for dirt, presumably thanks to its cohesive property. Figure 7 reveals that, to first order, loading efficiency, productivity, and load mass are linearly related, and they are positively correlated with the pile slope. However, many of the higher load mass cases are associated with poor productivity. The efficiency and productivity for dirt and sand have similar distributions, but higher load mass can be achieved with dirt. The efficiency and productivity are generally lower for gravel than for sand and dirt.

To study the sensitivity of action parameters, we select two performance points, $(\mathcal{P}_p, \mathcal{P}_e)$, in the gravel 30° data and extract the action parameter values that produce a similar performance. The performance of the identical set of action parameters on the five other sets of piles is then highlighted. The two performance points in gravel 30° are $(150, 8.0)$ and $(190, 9.0)$, and they are highlighted with $(\times)$ and $(+)$, respectively. The corresponding performance points are not gathered narrowly in the distributions for other pile angles but more so for dirt and sand piles with 30° slope. This suggests that loading actions should be adapted to the slope of the pile, while high-performing actions may transfer to piles of different material but similar slope.

A selection of points of special interest (POI) is made for each pile slope and material. These points correspond to maximum efficiency (○), productivity (△), load mass (□), and a Pareto optimal point (◇). The Pareto optimal point (◇) is chosen in between maximum efficiency (○) and productivity (△) randomly. The action parameters and performance values for the POI:s for 30° slopes are presented in Table 3. We observe that a high entry speed (α_1) and medium-high dig speed (α_2) are beneficial for high productivity while high efficiency relates to low dig speed (α_2). For large load mass, it appears important to trigger tilting at a large digging forces (α_4) and to tilt at low speed (α_6). No obvious relations are found for many of the action parameters and performance values.

Although it is in general not possible to control the bucket to follow a prescribed path, it is interesting to analyze the trajectories of the POI loadings. This is presented in Figure 8 and 9 for different slope and material, respectively. Also shown are the initial and resulting pile surfaces as well as the initial position of the mass that is loaded or just displaced by the loading action. At lower slope, in Figure 8, we note a larger tendency for soil being pushed forward and not ending up in the bucket, negatively affecting efficiency, productivity, and load mass. In Figure 9 the loadings of maximal mass (□) dig into the pile deep. However, it is not obvious that the feature of other loading types between each other.

5 Discussion

Overall, the admittance-like control method seems to work well if adjusted for the pile slope. The results suggest that the preferred digging actions should preserve and exploit a steep pile slope. It appears more important to adapt the loading actions to the pile shape than to the soil type, at least among the materials tested in this study. High digging speed favors high productivity, while energy-efficient loading requires a lower dig speed.

Several delimitations have been made in the present study, and many questions are left for future work. The effect of more complex pile shapes and other materials needs to be studied. The reason for the moderate load mass for gravel is not understood. Possibly the virtual gravel represents a more densely packed and stronger material than what was used in the field experiments. Also, from field tests, one expects a larger difference in the high-performance trajectories between the materials, e.g., longer, and more shallow digging for dirt than gravel and lower and more deep thrusting motions for sand. These tendencies are present for the high-productivity trajectories in Figure 9, but the difference is expected to be larger. Digging actions can be represented and discretized differently than in the present study, and it is certainly possible that higher performance loading can be discovered within the present action space. The spillage and resulting pile surface can be observed in the results, but we have not investigated how this penalizes sequential loadings.
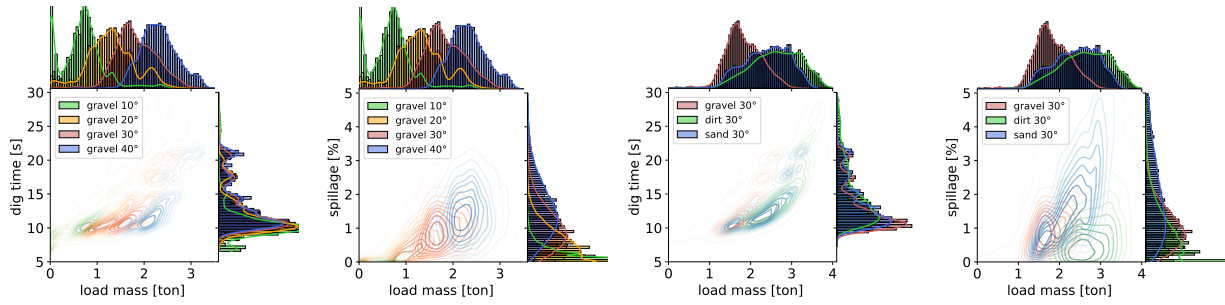
Figure 6. Distribution of loadings relative to mass, time, and spillage for different piles.

Table 3. Action parameters and performance for selected loadings on piles with 30° slope.

soil	loading	α_1	α_2	α_3	α_4	α_5	α_6	α_7	α_8	m_{load}	t_{load}	s_{load}	$\mathcal{P}_{prod}$	$\mathcal{P}_{eff}$
gravel	○	0.6	0.2	0.0	1.2	0.4	0.2	−30°	45°	3.40	24.5	1.5	139	**11.27**
gravel	△	0.8	0.4	0.0	0.9	0.6	1.0	−30°	30°	2.15	10.3	2.0	**207**	9.82
gravel	◇	0.6	0.4	0.0	1.2	0.4	0.6	−30°	30°	2.51	12.3	0.3	203	10.68
gravel	□	0.6	0.4	0.3	1.2	0.8	0.2	−30°	45°	**3.41**	25.1	2.4	136	10.53
dirt	○	0.6	0.2	0.0	0.9	0.8	1.0	−30°	30°	2.81	11.7	0.8	240	**11.80**
dirt	△	0.8	0.6	0.9	1.2	0.2	1.0	−40°	30°	2.92	11.3	0.0	**257**	11.13
dirt	◇	0.8	0.4	0.3	0.9	0.2	0.8	−30°	30°	2.76	11.2	1.3	245	11.14
dirt	□	0.6	0.4	0.3	1.2	0.6	0.2	−30°	45°	**4.12**	32.7	1.5	126	9.09
sand	○	0.8	0.2	0.0	0.9	1.0	1.0	−40°	30°	2.43	10.5	1.8	232	**12.16**
sand	△	0.8	0.6	0.6	0.3	0.2	0.8	−40°	45°	2.98	11.6	3.6	**257**	11.48
sand	◇	0.8	0.4	0.0	0.6	1.0	1.0	−30°	45°	2.80	11.2	4.9	248	11.83
sand	□	0.8	0.4	0.0	1.2	0.6	0.2	−30°	45°	**3.65**	25.5	5.5	143	10.12
										[ton]	[sec]	[%]	[kg/s]	[kg/kJ]

6   Conclusion

We have develope a simulator to explore the sequential loading actions which maximize the performance of automated wheel loader systems. The simulator is based on 3D multibody dynamics and deformable terrain with real-time capability. A vast number of loading simulations demonstrates that the combined action and pile state significantly affects the performance. As the next step, we will study the sequential loading scenario and address the optimization problem.

Acknowledgements

References

[1] A. Hemami and H. Ferri. An Overview of Autonomous Loading of Bulk Material. In *Proceedings of the 2009 International Symposium on Automation and Robotics in Construction (ISARC 2009)*, pages 405–411, Austin, USA, jun 2009. doi:10.22260/ISARC2009/0013.

[2] M. Servin, T. Berglund, and S. Nystedt. A multiscale model of terrain dynamics for real-time earthmoving simulation. *Advanced Modeling and Simulation in Engineering Sciences*, 8(1), 2021. doi:10.1186/s40323-021-00196-3.

[3] M. Shimizu and S. Matsumura. Productivity Improvement by Visualization of Construction Machinery Operation. Technical report, 2019. URL https://home.komatsu/en/company/tech-innovation/report/pdf/200331_04e.pdf.

[4] S. Singh and H. Cannon. Multi-resolution planning for earthmoving. In *Proceedings. 1998 IEEE International Conference on Robotics and Automation*, volume 1, pages 121–126, 1998. doi:10.1109/ROBOT.1998.676332.

[5] S. Sarata, Y. Weeramhaeng, and T. Tsubouchi. Planning of Scooping Position and Approach Path for Loading Operation by Wheel Loader. In *22nd International Symposium on*
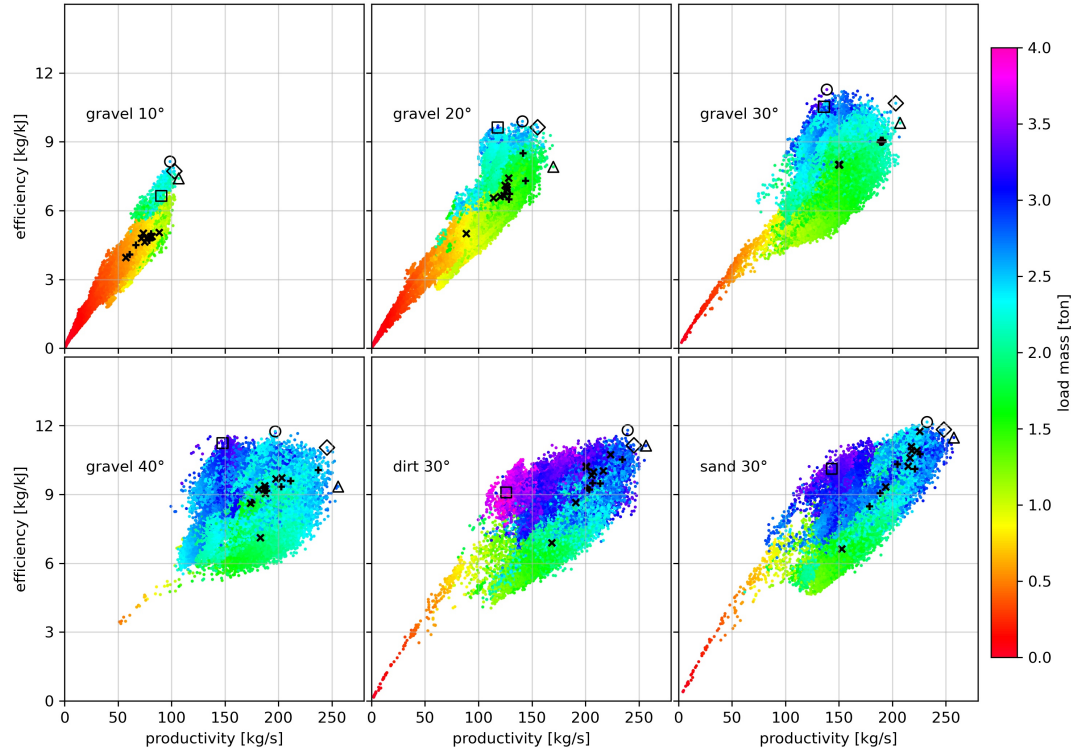
Figure 7. Distribution of the loading performance for each pile, marking some points of interest; the most efficient (○); productive (△); Pareto optimal (◇); and the highest load mass (□). Points highlighted with (+) and (×) are loadings performed with two nearly identical sets of action parameters selected from gravel 30°.
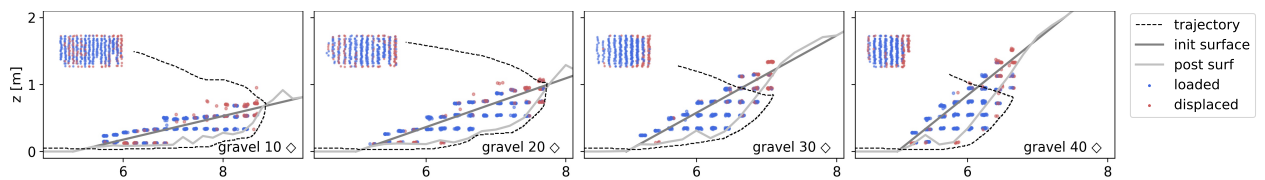

Figure 8. Bucket tip trajectories for Pareto optimal loadings from gravel piles with different slopes. The initial and resulting pile surface is shown as well as what mass is loaded successfully or just displaced, with the top view projection included in the upper left corners.
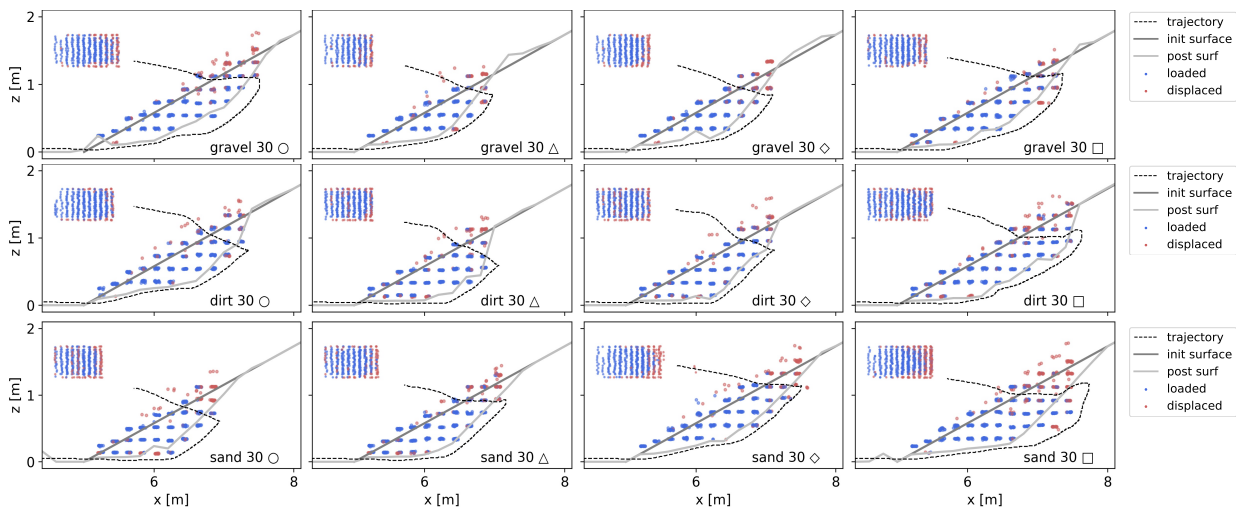
Figure 9. Bucket tip trajectories for 30° piles of different material (row) and the four different loading performance POI (column). The initial and resulting pile surface is shown as well as what mass is loaded successfully or just displaced, with the top view projection included in the upper left corners.

Automation and Robotics in Construction, 2005. doi:10.22260/ISARC2005/0079.

[6] R. Filla, M. Obermayr, and B. Frank. A study to compare trajectory generation algorithms for automatic bucket filling in wheel loaders. In K Berns, C Schindler, and K Dressler, editors, *Commercial Vehicle Technology: Proceedings of the 3rd Commercial Vehicle Technology Symposium (CVT 2014)*, 2014.

[7] R. Filla and B. Frank. Towards Finding the Optimal Bucket Filling Strategy through Simulation. In *The 15th Scandinavian International Conference on Fluid Power*, 2017. doi:10.3384/ecp17144402.

[8] D. Lindmark and M. Servin. Computational exploration of robotic rock loading. *Robotics and Autonomous Systems*, 106:117–129, 2018. doi:https://doi.org/10.1016/j.robot.2018.04.010.

[9] S. Dadhich, F. Sandin, U. Bodin, U. Andersson, and T. Martinsson. Field test of neural-network based automatic bucket-filling algorithm for wheel-loaders. *Automation in Construction*, 97:1–12, 2019. doi:https://doi.org/10.1016/j.autcon.2018.10.013. URL http://www.sciencedirect.com/science/article/pii/S0926580518305119.

[10] D. Bradley and D. Seward. The development, control and operation of an autonomous robotic excavator. *Journal of Intelligent and Robotic Systems*, 21(1): 73–97, 1998. doi:10.1023/A:1007932011161.

[11] Algoryx Simulations. AGX Dynamics, August 2021. URL https://www.algoryx.se/products/agx-dynamics/.

[12] M. Oba. Introduction of Products Introduction of Small-Size Wheel Loaders WA270-7 and WA320-7. *KOMATSU TECHNICAL REPORT*, 59(166):1–7, 2013.

[13] Komatsu WA320-7 Specifications and Technical Data, 2014. URL https://www.komatsu.eu/Assets/GetBrochureByProductName.aspx?id=WA320-7&langID=en.

[14] A. Dobson, J. Marshall, and J. Larsson. Admittance control for robotic loading: Design and experiments with a 1-tonne loader and a 14-tonne load-haul-dump machine. *Journal of Field Robotics*, 34(1):123–150, 2017.